Fast Directional Spatially Localized Spherical Harmonic Transform

Zubair Khalid, *Student Member, IEEE*, Rodney A. Kennedy, *Fellow, IEEE*, Salman Durrani, *Senior Member, IEEE*, Parastoo Sadeghi, *Senior Member, IEEE*, Yves Wiaux, *Member, IEEE*, and Jason D. McEwen, *Member, IEEE*

Abstract—We propose a transform for signals defined on the sphere that reveals their localized directional content in the spatio-spectral domain when used in conjunction with an asymmetric window function. We call this transform the directional spatially localized spherical harmonic transform (directional SLSHT) which extends the SLSHT from the literature whose usefulness is limited to symmetric windows. We present an inversion relation to synthesize the original signal from its directional-SLSHT distribution for an arbitrary window function. As an example of an asymmetric window, the most concentrated band-limited eigenfunction in an elliptical region on the sphere is proposed for directional spatio-spectral analysis and its effectiveness is illustrated on the synthetic and Mars topographic data-sets. Finally, since such typical data-sets on the sphere are of considerable size and the directional SLSHT is intrinsically computationally demanding depending on the band-limits of the signal and window, a fast algorithm for the efficient computation of the transform is developed. The floating point precision numerical accuracy of the fast algorithm is demonstrated and a full numerical complexity analysis is presented.

Index Terms—Signal analysis, spherical harmonics, 2-sphere.

I. INTRODUCTION

SIGNALS that are inherently defined on the sphere appear in various fields of science and engineering, such as medical image analysis [1], geodesy [2], computer graphics [3], planetary science [4], electromagnetic inverse problems [5], cosmology [6], 3D beamforming [7] and wireless channel modeling [8]. In order to analyze and process signals on the sphere, many signal processing techniques have been extended

from the Euclidean domain to the spherical domain [2], [9]–[23].

Due to the ability of wavelets to resolve localized signal content in both space and scale, wavelets have been extensively investigated for analyzing signals on the sphere [9], [13]–[15], [19]–[23] and have been utilized in various applications (e.g., in astrophysics [24]–[29] and geophysics [4], [30], [31]). Some of the wavelet techniques on the sphere also incorporate directional phenomena in the spatial-scale decomposition of a signal (e.g., [21]–[23]). As an alternative to spatial-scale decomposition, spatio-spectral (spatial-spectral) techniques have also been developed and applied for localized spectral analysis, spectral estimation and spatially varying spectral filtering of signals [10], [12], [18], [32], [33]. The spectral domain is formed through the spherical harmonic transform which serves as a counterpart of the Fourier transform for signals on the sphere [5], [34]–[36].

The localized spherical harmonic transform, composed of spatial windowing followed by spherical harmonic transform, was first devised in [18] for localized spectral analysis. We note that the localized spherical harmonic transform was defined in [18] for azimuthally asymmetric (i.e., directional) window functions, however, it was applied and investigated for azimuthally symmetric functions only. Furthermore, a spectrally truncated azimuthally symmetric window function was used for spatial localization [18]. Due to spectral truncation, the window used for spatial localization may not be concentrated in the region of interest. This issue was resolved in [32], where azimuthally symmetric eigenfunctions obtained from the Slepian concentration problem on the sphere were used as window functions (the Slepian concentration problem is studied for arbitrary regions on the sphere in [2]). Following [18], the spatially localized spherical harmonic transform (SLSHT) for signals on the sphere has been devised in [10] to obtain the spatio-spectral representation of signals for azimuthally symmetric window functions, where the effect of different window functions on the SLSHT distribution is studied. Subsequently, the SLSHT has been used to perform spatially varying spectral filtering [12], again with azimuthally symmetric window functions.

In obtaining the SLSHT distribution for spatio-spectral representation of a signal, the use of an azimuthally symmetric window function provides mathematical simplifications. However, such an approach cannot discriminate localized directional features in the spatio-spectral domain. This motivates the use of asymmetric window functions in the spatio-spectral transformation of a signal using the SLSHT. In order to

serve this objective, we employ the definition of the localized spherical harmonic transform in [18] and define the SLSHT and the SLSHT distributions using azimuthally asymmetric window functions for spatial localization. Since the use of an asymmetric window function enables the transform to reveal directional features in the spatio-spectral domain, we call the proposed transform the directional SLSHT. We also provide a harmonic analysis of the proposed transform and present an inversion relation to recover the signal from its directional SLSHT distribution.

Since the directional SLSHT distribution of a signal is required to be computed for each spatial position and for each spectral component, and data-sets on the sphere are of considerable size (e.g., three million samples on the sphere for current data-sets [37] and fifty million samples for forthcoming data-sets [38]), the evaluation of the directional SLSHT distribution is computationally challenging. We develop fast algorithms for this purpose. Through experimental results we show the numerical accuracy and efficient computation of the proposed directional SLSHT transform. Furthermore, due to the fact that the proposed directional SLSHT distribution depends on the window function used for spatial localization, we analyze the asymmetric band-limited window function with nominal concentration in an elliptical region around the north pole, which is obtained from the Slepian concentration problem on the sphere. We also illustrate, through an example, the capability of the proposed directional SLSHT to reveal directional features in the spatio-spectral domain.

The remainder of the paper is structured as follows. In Section II, we review mathematical preliminaries related to the signals on the sphere, which are required in the sequel. We present the formulation of the directional SLSHT, its harmonic analysis and signal reconstruction from the SLSHT distribution in Section III. Different algorithms for the evaluation of the SLSHT distribution are provided in Section IV. In Section V, we show timing and accuracy results of our algorithms and an illustration of the transform. Concluding remarks are presented in Section VI.

II. MATHEMATICAL BACKGROUND

In order to clarify the adopted notation, we review some mathematical background for signals defined on the sphere and the rotation group.

A. Signals on the Sphere

In this work, we consider the square integrable complex functions $f(\hat{\boldsymbol{x}})$ defined on unit sphere $\mathbb{S}^2 \triangleq \{\mathbf{u} \in \mathbb{R}^3 : |\mathbf{u}| = 1\}$, where $|\cdot|$ denotes Euclidean norm, $\hat{\boldsymbol{x}} \equiv \hat{\boldsymbol{x}}(\theta, \phi) \triangleq (\sin\theta\cos\phi, \ \sin\theta\sin\phi, \ \cos\theta)^T \ \in \mathbb{R}^3$ is a unit vector and parameterizes a point on the unit sphere with $\theta \in [0, \pi]$ denoting the co-latitude and $\phi \in [0, 2\pi)$ denoting the longitude. The inner product of two functions f and h on $\mathbb{S}^2$ is defined as [39]

$$\langle f, h \rangle \triangleq \int_{\mathbb{S}^2} f(\hat{\boldsymbol{x}})\overline{h(\hat{\boldsymbol{x}})} \, ds(\hat{\boldsymbol{x}}), \qquad (1)$$

where $\overline{(\cdot)}$ denotes the complex conjugate, $ds(\hat{\boldsymbol{x}}) = \sin\theta d\theta d\phi$ and the integration is carried out over the unit sphere. With the

inner product in (1), the space of square integrable complex valued functions on the sphere forms a complete Hilbert space $L^2(\mathbb{S}^2)$. Also, the inner product in (1) induces a norm $\|f\| \triangleq \langle f, f \rangle^{1/2}$. We refer the functions with finite induced norm as signals on the sphere.

The Hilbert space $L^2(\mathbb{S}^2)$ is separable and the spherical harmonics form the archetype complete orthonormal set of basis functions. The spherical harmonics, $Y_\ell^m(\hat{\boldsymbol{x}}) = Y_\ell^m(\theta, \phi)$, for degree $\ell \geq 0$ and order $|m| \leq \ell$ are defined as [5], [36]

$$Y_\ell^m(\theta, \phi) = N_\ell^m \, P_\ell^m(\cos\theta)e^{im\phi}, \qquad (2)$$

where $N_\ell^m = \sqrt{\frac{2\ell+1}{4\pi}\frac{(\ell-m)!}{(\ell+m)!}}$ denotes the normalization constant and P_ℓ^m are the associated Legendre polynomials [36]. With the above definitions, the spherical harmonics form an orthonormal set of basis functions, i.e., they satisfy $\langle Y_\ell^m, Y_{\ell'}^{m'} \rangle = \delta_{\ell\ell'}\delta_{mm'}$, where $\delta_{\ell\ell'}$ is the Kronecker delta.

By completeness and orthonormality of the spherical harmonics, we can expand any signal $f \in L^2(\mathbb{S}^2)$ as

$$f(\hat{\boldsymbol{x}}) = \sum_{\ell=0}^{\infty} \sum_{m=-\ell}^{\ell} \left(f\right)_\ell^m Y_\ell^m(\hat{\boldsymbol{x}}), \qquad (3)$$

where

$$\left(f\right)_\ell^m \triangleq \langle f, Y_\ell^m \rangle = \int_{\mathbb{S}^2} f(\hat{\boldsymbol{x}})\overline{Y_\ell^m(\hat{\boldsymbol{x}})} \, ds(\hat{\boldsymbol{x}}) \qquad (4)$$

denotes the spherical harmonic coefficient of degree ℓ and order m. The signal f is said to be band-limited with maximum spherical harmonic degree L_f if $\left(f\right)_\ell^m = 0, \ \forall \ell > L_f$.

B. Rotations on the Sphere and Wigner-D Functions

Rotations on the sphere are often parameterized using Euler angles $(\alpha, \beta, \gamma) \in \mathrm{SO}(3)$, where $\alpha \in [0, 2\pi)$, $\beta \in [0, \pi]$ and $\gamma \in [0, 2\pi)$ [36]. Using the 'zyz' Euler convention, we define the rotation operator $\mathscr{D}_\rho$, for $\rho = (\alpha, \beta, \gamma) \in \mathrm{SO}(3)$, which rotates a function on a sphere in the sequence of γ rotation around z-axis, then β rotation about y-axis followed by a α rotation around z-axis. The spherical harmonic coefficient of a rotated signal $\mathscr{D}_\rho f$ is related to the coefficients of the original signal by

$$\left(\mathscr{D}_\rho f\right)_\ell^m = \sum_{m'=-\ell}^{\ell} D_{m,m'}^\ell(\rho)\left(f\right)_\ell^{m'}, \ \rho = (\alpha, \beta, \gamma), \qquad (5)$$

where $D_{m,m'}^\ell(\rho)$ denotes the Wigner-D function [36] of degree ℓ and orders m and m' and is given by

$$\begin{aligned} D_{m,m'}^\ell(\rho) &= D_{m,m'}^\ell(\alpha, \beta, \gamma) \qquad (6) \\ &= e^{-im\alpha}d_{m,m'}^\ell(\beta) \, e^{-im'\gamma}, \ \rho = (\alpha, \beta, \gamma), \end{aligned}$$

where $d_{m,m'}^\ell(\beta)$ is the Wigner-d function [36].

C. Signals on the Rotation Group SO(3)

For $\ell \geq 0$ and $m, m' \in \mathbb{Z}$ such that $|m|, |m'| \leq \ell$, the Wigner-D functions in (6) form a complete set of orthogonal

functions for the space $L^2(\text{SO}(3))$ of functions defined on the rotation group SO(3) and follow the orthogonality relation

$$\int_{\text{SO}(3)} D_{m,m'}^\ell(\rho)\overline{D_{q,q'}^p(\rho)}\, d\rho = \frac{8\pi^2}{2\ell+1}\,\delta_{\ell p}\delta_{mq}\delta_{m'q'}, \qquad (7)$$

where $d\rho = d\alpha\sin\beta d\beta d\gamma$ and the integral is a triple integral over all rotations $(\alpha,\beta,\gamma) \in \text{SO}(3)$ [36]. Thus, any function $f \in L^2(\text{SO}(3))$ may be expressed as

$$f(\rho) = \sum_{\ell=0}^\infty \sum_{m=-\ell}^\ell \sum_{m=-\ell'}^{\ell'} (f)_{m,m'}^\ell D_{m,m'}^\ell(\rho), \qquad (8)$$

where

$$(f)_{m,m'}^\ell = \frac{2\ell+1}{8\pi^2}\int_{\text{SO}(3)} f(\rho)\overline{D_{m,m'}^\ell(\rho)}\, d\rho. \qquad (9)$$

The signal f is said to be band-limited with maximum degree L_f if $(f)_{m,m'}^\ell = 0, \forall \ell > L_f$.

D. Discretization of $\mathbb{S}^2$ and SO(3)

In order to represent functions on $\mathbb{S}^2$ and SO(3), it is necessary to adopt appropriate tessellation schemes to discretize both the unit sphere domain and the Euler angle domain of SO(3). We consider tessellation schemes that support a sampling theorem for band-limited functions, which is equivalent to supporting an exact quadrature.

For the unit sphere domain, we adopt the equiangular tessellation scheme [35] defined as $\mathfrak{S}_L = \{\theta_{n_\theta} = \pi(2n_\theta+1)/(2L+1), \phi_{n_\phi} = 2\pi n_\phi/(2L+1) : 0 \le n_\theta \le L, 0 \le n_\phi \le 2L\}$, which is a grid of $(L+1)\times(2L+1)$ sample points on the sphere (including repeated samples of the south pole) that keeps the sampling in θ and ϕ independent. For a band-limited function on the sphere $f \in L^2(\mathbb{S}^2)$ with maximum spherical harmonic degree L_f, the sampling on the grid $\mathfrak{S}_{L_f}$ ensures that all information of the function is captured in the finite set of samples and, moreover, that exact quadrature can be performed [35]. Note that this sampling theorem was developed only recently [35] and requires approximately half as many samples on the sphere as required by alternative equiangular sampling theorems on the sphere [34].

For the Euler angle representation of the rotation group SO(3), we consider the equiangular tessellation scheme $\mathfrak{E}_L = \{\alpha_{n_\alpha} = 2\pi n_\alpha/(2L+1), \beta_{n_\beta} = 2\pi n_\beta/(2L+1), \gamma_{n_\gamma} = 2\pi n_\gamma/(2L+1) : 0 \le n_\alpha, n_\gamma \le 2L, 0 \le n_\beta \le L\}$. Again for a function $f \in L^2(\text{SO}(3))$ with maximum spectral degree L_f, the sampling of a function f on $\mathfrak{E}_{L_f}$ ensures that all information of the function is captured and also permits exact quadrature (which follows from the results developed on the sphere [35]).

III. DIRECTIONAL SLSHT

We describe in this section the directional SLSHT, which is capable of revealing directional features of signals in the spatio-spectral[1] domain. For spatial localization, we consider

[1]When we refer to spatio-spectral, we consider the SO(3) spatial domain, instead of $\mathbb{S}^2$. This is due to the reason that we are considering all possible rotations, parameterized using Euler angles which form the SO(3) domain.

the band-limited azimuthally asymmetric window function which is spatially concentrated in some asymmetric region around the north pole. Since the rotation around the z-axis does not have any affect on an azimuthally symmetric function, the localized spherical harmonic transform using an azimuthally symmetric window function can be parameterized on the sphere. However, if an azimuthally asymmetric window is used to obtain localization in the spatial domain, the rotation of the window function is fully parameterized with the consideration of all three Euler angles $(\alpha,\beta,\gamma) \in \text{SO}(3)$. We refer to the spatially localized transform using an asymmetric window as the directional SLSHT. Here, we first define the directional SLSHT distribution which presents the signal in the spatio-spectral domain. Later in this section, we present the harmonic analysis of SLSHT distribution and provide an inversion relation to obtain the signal from its given directional SLSHT distribution.

A. Forward Directional SLSHT

Definition 1 (Directional SLSHT): For a signal $f \in L^2(\mathbb{S}^2)$, define the directional SLSHT distribution component $g(\rho;\ell,m) \in L^2(\text{SO}(3))$ of degree ℓ and order m as the spherical harmonic transform of a localized signal where localization is provided by the rotation operator $\mathscr{D}_\rho$ acting on window function $h \in L^2(\mathbb{S}^2)$, i.e.,

$$g(\rho;\ell,m) \triangleq \int_{\mathbb{S}^2} f(\hat{\boldsymbol{x}})\,(\mathscr{D}_\rho h)(\hat{\boldsymbol{x}})\,\overline{Y_\ell^m(\hat{\boldsymbol{x}})}\, ds(\hat{\boldsymbol{x}}) \qquad (10)$$

for $0 \le \ell \le L_g$, $|m| \le \ell$, where $L_g = L_f + L_h$ denotes the maximum spherical harmonic degree for which the distribution components $g(\rho;\ell,m)$ are non-zero, and L_f and L_h denote the band-limits of the signal f and the window function h, respectively. Also, each distribution component $g(\rho;\ell,m)$ is band-limited in $\rho = (\alpha,\beta,\gamma) \in \text{SO}(3)$ with maximum degree L_h, i.e., when expressed in terms of Wigner-D functions. We elaborate on this shortly. Furthermore, we consider unit energy normalized window functions such that $\langle h, h \rangle = 1$.

Remark 1: The directional SLSHT distribution component in (10) can be interpreted as the spherical harmonic transform of the localized signal where the window function h provides asymmetric localization at spatial position $\hat{\boldsymbol{x}} = \hat{\boldsymbol{x}}(\beta,\alpha) \in \mathbb{S}^2$ and the first rotation, through γ, determines the orientation of the window function at $\hat{\boldsymbol{x}}$. If the window function is azimuthally symmetric, this orientation of the window function by γ becomes invariant and the SLSHT distribution components are defined on $L^2(\mathbb{S}^2)$ [10].

Since the maximum spectral degree for which the SLSHT distribution is defined is $L_g = L_f + L_h$, we consider the band-limited window function such that $L_h \le L_f$ to avoid extending L_g significantly above L_f. We discuss the localization of the window function in spatial and spectral domains later in the paper.

B. Harmonic Analysis

We now present the formulation of the directional SLSHT distribution if the signal f and the window function h are represented in the spectral domain. Using the expression of

the spherical harmonics of a rotated function in (5), we can write the SLSHT distribution component $g(\rho; \ell, m)$ in (10) as

$$g(\rho; \ell, m) = \sum_{\ell'=0}^{L_f} \sum_{m'=-\ell'}^{\ell'} (f)_{\ell'}^{m'} \qquad (11)$$

$$\times \sum_{p=0}^{L_h} \sum_{q=-p}^{p} \sum_{q'=-p}^{p} (h)_p^{q'} D_{q,q'}^p(\rho) T(\ell', m'; p, q; \ell, m),$$

where

$$T(\ell', m'; p, q; \ell, m) = \int_{\mathbb{S}^2} Y_{\ell'}^{m'}(\hat{\boldsymbol{x}}) Y_p^q(\hat{\boldsymbol{x}}) \overline{Y_\ell^m(\hat{\boldsymbol{x}})} \, ds(\hat{\boldsymbol{x}})$$

denotes the spherical harmonic triple product, which can be evaluated using Wigner-$3j$ symbols or Clebsch-Gordan coefficients [36], [40].

Remark 2: By comparing $g(\rho; \ell, m)$ in (11) with (8), we note that the band-limit of $g(\rho; \ell, m)$ in ρ is given by L_h. Since $\ell' \leq L_f$ and $p \leq L_h$ in (11), our statement that the distribution component $g(\rho; \ell, m)$ is non-zero for $\ell \leq L_g = L_f + L_h$ follows since the triple product $T(\ell', m'; p, q; \ell, m)$ is non-zero for $\ell \leq L_f + L_h$ only.

C. Inverse Directional SLSHT

Here, we define the inverse directional SLSHT to reconstruct a signal from its SLSHT distribution. The original signal can be reconstructed from its directional SLSHT distribution through the spectral domain marginal, that is, by integrating the SLSHT distribution components over the spatial domain SO(3) [18]. Using our harmonic formulation in (11), define $(\hat{f})_\ell^m$ as the integral of the SLSHT distribution component $g(\rho; \ell, m)$ over SO(3) giving

$$(\hat{f})_\ell^m = \int_{\text{SO(3)}} g(\rho; \ell, m) d\rho, \quad 0 \leq \ell \leq L_f$$

$$= \sum_{\ell'=0}^{L_h} \sum_{m'=-\ell'}^{\ell'} (f)_{\ell'}^{m'} \sum_{p=0}^{L_h} \sum_{q=-p}^{p} \sum_{q'=-p}^{p} (h)_p^{q'}$$

$$\times T(\ell', m'; p, q; \ell, m) \int_{\text{SO(3)}} D_{q,q'}^p(\rho) \, d\rho$$

$$= \sqrt{16\pi^3} (h)_0^0 (f)_\ell^m, \qquad (12)$$

where we have used the orthogonality relation of Wigner-D functions (see (7)). Using the expression in (12), we can find the spherical harmonic coefficient $(f)_\ell^m$ of the signal f as

$$(f)_\ell^m = \frac{(\hat{f})_\ell^m}{\sqrt{16\pi^3} (h)_0^0}, \qquad (13)$$

which indicates that we only need to know the DC component of the window function $(h)_0^0$ in order to obtain the signal from its directional SLSHT distribution. It further imposes the condition that the DC component of the window function must be non-zero. Although the distribution components in (11) are defined up to degree $L_g = L_f + L_h$, we only require the components up to L_f for signal reconstruction.

Remark 3: The signal can also be reconstructed from its SLSHT distribution by evaluating

$$\int_{\text{SO(3)}} g(\rho; \ell, m) \overline{D_{q,q'}^p(\rho)} d\rho = 8\pi^2 \sum_{\ell'=0}^{L_h} \sum_{m'=-\ell'}^{\ell'} (f)_{\ell'}^{m'} \sum_{p=0}^{L_h} \sum_{q=-p}^{p}$$

$$\times \sum_{q'=-p}^{p} \frac{(h)_p^{q'}}{2p+1} T(\ell', m'; p, q; \ell, m)$$

for all $p \leq L_h$, $|q|, q' | \leq p$ and for all $\ell \leq L_g$, $|m| \leq \ell$ and then employing the orthogonality relations of Wigner-$3j$ symbols to decouple the spherical harmonic coefficients of the window function h and the signal f. The similar approach has been employed in [12] to invert the signal from its modified SLSHT distribution, where the SLSHT distribution is obtained using azimuthally symmetric window function. This approach does not impose restriction on the DC component of the window function to be non-zero, instead, it requires the knowledge of the energy of the window function. In this work, we consider the inversion of a signal presented in (12) and (13), as this is the most efficient formulation.

Computing the forward and inverse directional SLSHT is computationally demanding. Since the directional SLSHT distribution components $g(\rho; \ell, m)$ in (10) are defined for $\ell \leq L_g$, the number of distribution components are of the order L_g^2, while the sampling of ρ is of the order L_h^3; thus, the direct evaluation of the directional SLSHT distribution is prohibitively computationally expensive. Therefore efficient algorithms need to be developed which reduce the computational complexity. We address this problem in the next section.

D. Window localization in Spatial and Spectral Domains

The directional SLSHT distribution is the spherical harmonic transform of the product of two functions, the signal f and the rotated window function h and we must be careful in interpreting the directional SLSHT distribution in the sense that we do not mistake using the signal to study the window because there is no distinction mathematically. The window function should be chosen so that it provides spatial localization in some spatial region around the north pole (origin). Since we have considered a band-limited window function, the window function cannot be perfectly localized in the spatial domain due to the uncertainty principle on the sphere [41]. However, it can be optimally localized by maximizing the energy concentration of the window function in the desired directional region [2].

The interpretation and the effectiveness of the directional SLSHT distribution depends on the chosen window function. The window function with maximum localization in some defined asymmetric region provides directional localization and thus reveals directional features in the spatio-spectral domain. The more directional the window function, the more directional features it can reveal in the spatio-spectral domain but this tends to increase the maximum spherical harmonic degree L_h. Recall that the maximum degree of the directional SLSHT distribution components is given by $L_g = L_f + L_h$. Thus, when the signal is expressed in the spatio-spectral

domain its spectral domain is extended by L_h, which results in spectral leakage. Therefore, we want the window function to be simultaneously maximally localized in some spatial region $\mathscr{R} \subset \mathbb{S}^2$ and have the minimum possible band-limit which achieves the desired level of energy concentration in the spatial region $\mathscr{R}$.

With the consideration that there exists localization trade-off for a window function in spatial and spectral domain [41], the choice of window function affects the resulting SLSHT distribution. We highlight the future research problem that there is a need to investigate the use of different window function at different spatial positions, such that the localization of the window function adapts to the characteristics of the signal being analyzed. An analogous problem is well known in time-frequency analysis [42], where it has been shown that, according to several different measures of performance, the optimal window function for short-time Fourier transform (STFT) depends on the signal being analyzed.

Here, we propose using a band-limited eigenfunction obtained from the solution of the Slepian concentration problem [2] as a window function, concentrated in a spatially localized elliptical region around the north pole. The elliptical region can be parameterized using the focus colatitude θ_c of the ellipse along the positive x-axis and the arc length a of the semi-major axis:

$$\mathscr{R}_{(\theta_c, a)} \triangleq \big\{ (\theta, \phi) : \triangle_s\big((\theta, \phi), (\theta_c, 0)\big)$$
$$+ \triangle_s\big((\theta, \phi), (\theta_c, \pi)\big) \leq 2a \big\}, \quad (14)$$

where $0 \leq \theta_c \leq a \leq \pi/2$. Here $\triangle_s\big((\theta, \phi), (\theta', \phi')\big) = \arccos\big(\sin\theta \sin\theta' \cos(\phi - \phi') + \cos\theta \cos\theta'\big)$ denotes the angular distance between two points (θ, ϕ) and (θ', ϕ') on the sphere. Since the major axis is along x-axis, the elliptical region is orientated along the x-axis.

Remark 4: For a given focus θ_c, the region becomes more directional as the arc length a approaches θ_c from $\pi/2$. For $a = \pi/2$, the region becomes azimuthally symmetric, i.e., we recover the polar cap of central angle $\pi/2$. Also, when $\theta_c = 0$, the region becomes azimuthally symmetric (polar cap) of central angle a.

As a result of the Slepian concentration problem [2], [43] to find the band-limited function with bandwidth L_h and maximal spatial concentration in an elliptical region $\mathscr{R}_{(\theta_c, a)}$, we obtain $(L_h + 1)^2$ eigenfunctions. Due to the symmetry of the elliptical region about x-y plane, the eigenfunctions are real valued [43]. Here we consider the use of the band-limited eigenfunction with maximum energy concentration in the elliptical region for given band-limit L_h and refer to such an eigenfunction as the eigenfunction window.

IV. EFFICIENT COMPUTATION OF DIRECTIONAL SLSHT DISTRIBUTION

Here, we present efficient algorithms for the computation of the directional SLSHT distribution of a signal and the signal reconstruction from its directional SLSHT distribution. First, we discuss the computational complexities if the SLSHT distribution components are computed using direct quadrature as given in (10) or using the harmonic formulation in (11).

Later, we develop an alternative harmonic formulation which reduces the computational burden. Finally, we present an efficient algorithm that incorporates a factoring of rotations [44] and exploits the FFT.

First we need to parameterize the required tessellation schemes for $\mathbb{S}^2$ for the representation of the signal f and the window h and for SO(3) which forms the spatial domain of the directional SLSHT distribution. Since the maximum spectral degree of the signal f is L_f, we therefore consider the equiangular tessellation $\mathfrak{S}_{L_f}$ to represent f. Since the maximum degree for all SLSHT distribution components $g(\rho; \ell, m)$ in ρ is L_h, we therefore consider the tessellation $\mathfrak{E}_{L_h}$ to represent the SLSHT distribution components on $L^2(\text{SO}(3))$.

A. Direct Quadrature and Harmonic Formulation

We define the forward spatio-spectral transform as evaluation of each SLSHT distribution component $g(\rho; \ell, m)$. Evaluation of the forward spatio-spectral transform using exact quadrature in (10) requires the computation of two dimensional summation over the tessellation of $\mathbb{S}^2$ for each 3-tuple (α, β, γ). Since there are $O(L_h^3)$ such 3-tuples in the tessellation scheme $\mathfrak{E}_{L_h}$ and the SLSHT distribution components are of the order $O(L_f^2)$, the computational complexity to compute all distribution components using direct quadrature is $O(L_f^4 L_h^3)$. Using the harmonic formulation in (11), the complexity to compute each SLSHT distribution component is $O(L_f^2 L_h^6)$ and to compute all SLSHT distribution components is $O(L_f^4 L_h^6)$. Although the harmonic formulation in (11) is useful to establish that the signal can be reconstructed from the directional SLSHT distribution, it is much more computationally demanding than direct quadrature. We develop efficient algorithms in the next subsection which improve the computational complexity of the harmonic formulation and make it more efficient than direct quadrature.

For the inverse directional SLSHT distribution, we only need to integrate over SO(3) to obtain the signal in the spherical harmonic domain as proposed in (12). Since the integral can be evaluated by a summation over all Euler angles using quadrature weights, an efficient way to recover the signal from its SLSHT distribution is through direct quadrature, with complexity of $O(L_h^3)$ for each distribution component and $O(L_f^2 L_h^3)$ for all components.

In order to evaluate the integral in (12) exactly, we need to define quadrature weights along Euler angle β in the tessellation $\mathfrak{E}_{L_h}$. We evaluate the integral in (12) by the following summation[2]

$$(\hat{f})_\ell^m = \frac{1}{(2L_h + 1)^3} \sum_{n_\alpha = 0}^{2L_h} \sum_{n_\beta = 0}^{L_h} \sum_{n_\gamma = 0}^{2L_h}$$
$$\times g(\alpha_{n_\alpha}, \beta_{n_\beta}, \gamma_{n_\gamma}; \ell, m) \, q(\beta_{n_\beta}), \quad (15)$$

[2]In the evaluation of (15) we have computed the summation over $2L_h + 1$ sample points in both α and γ. This is due to the tessellation $\mathfrak{E}_{L_h}$ required to capture all information content of $g(\alpha, \beta, \gamma; \ell, m)$. However, if one were considered in recovering f only, then given the quadrature rule in [35] $(\hat{f})_\ell^m$ in (15) could be computed exactly with only $L_h + 1$ sample points in α and γ.

where the quadrature weights $q(\beta_{n_\beta})$ follow from [35], with

$$q(\beta_{n_\beta}) = \begin{cases} 4\pi^2 \left(\lfloor \frac{L_h}{2} \rfloor + \frac{1}{2} \right)^{-1}, & \beta_{n_\beta} = 0 \\ 8\pi^2 \sum_{m=-L_h}^{L_h} w(-m) \cos m\beta_{n_\beta}, & \text{otherwise} \end{cases}$$

(16)

where $w(m)$ is defined as [35]

$$w(m) = \begin{cases} \frac{\pm i\pi}{2}, & m = \pm 1, \\ 0, & m \text{ odd}, m \neq 1, \\ \frac{2}{1-m^2}, & m \text{ even.} \end{cases}$$

(17)

B. Fast Algorithm for Forward Directional SLSHT

Here, we develop a fast algorithm to reduce the computational complexity of the forward SLSHT. We first consider an alternative harmonic formulation of the forward SLSHT and then employ the factoring of rotations approach which was first proposed in [44] and has been used in the implementations of the fast spherical convolution [45] and the directional spherical wavelet transform [15].

We may write the directional SLSHT distribution component $g(\rho; \ell, m)$ in (10) as a spherical convolution [15] of h and the spherical harmonic modulated signal $\overline{f} Y_\ell^m$, giving

$$g(\rho; \ell, m) = \sum_{p=0}^{L_h} \sum_{q=-p}^{p} \sum_{q'=-p}^{p} \overline{\left(\overline{f} Y_\ell^m\right)_p^q} (h)_p^{q'} D_{q,q'}^p(\alpha, \beta, \gamma),$$

(18)

which can be expressed, using the definition of the Wigner-D function in (6), as

$$g(\rho; \ell, m) = \sum_{p=0}^{L_h} \sum_{q=-p}^{p} \sum_{q'=-p}^{p} \overline{\left(\overline{f} Y_\ell^m\right)_p^q} \times (h)_p^{q'} d_{q,q'}^p(\beta) e^{-iq'\gamma} e^{-iq\alpha}.$$

(19)

The band-limit of the spherical harmonic modulated signal $\overline{f} Y_\ell^m$ is $L_f + \ell$. Since the maximum ℓ for which g is non-zero is $L_f + L_h$, we must compute up to $\overline{f} Y_{L_f+L_h}^m$, which is band-limited to $2L_f + L_h$. However, we *only* need to compute the spherical harmonic coefficients $\left(\overline{f} Y_\ell^m\right)_p^q$ of the modulated signal up to degree $p \leq L_h$. Therefore, the computation of the spherical harmonic transform of $\overline{f} Y_\ell^m$ is an interesting subproblem. We show in Appendix A that the spherical harmonic coefficients $\overline{\left(\overline{f} Y_\ell^m\right)_p^q}$ for $0 \leq p \leq L_h$, $|q| \leq p$ of the signal $\overline{f} Y_\ell^m$ can be computed in $O(L_f^3 L_h^2)$ time for all ℓ and m.

By factoring the single rotation by (α, β, γ) into two rotations [15], [44], [45]

$$\mathscr{D}_\rho = \mathscr{D}_{\rho_1} \mathscr{D}_{\rho_2}, \quad \rho = (\alpha, \beta, \gamma), \rho_1 = (\alpha - \pi/2, -\pi/2, \beta), \\ \rho_2 = (0, \pi/2, \gamma + \pi/2),$$

(20)

and noting the effect of rotation on spherical harmonic coefficients in (5), we can write the Wigner-D function in (6) as

$$D_{q,q'}^p(\alpha, \beta, \gamma) = i^{q-q'} \sum_{q''=-p}^{p} \Delta_{q''q}^p \Delta_{q''q'}^p e^{-iq\alpha - iq''\beta - iq'\gamma},$$

(21)

where $\Delta_{qq'}^p = d_{q,q'}^p(\pi/2)$ and we have used the following symmetry properties of Wigner-d functions [40]

$$d_{q,q'}^p(\beta) = (-1)^{q-q'} d_{q,q'}^p(-\beta) = (-1)^{q-q'} d_{-q,-q'}^p(\beta) \\ = (-1)^{q-q'} d_{q',q}^p(\beta) = d_{-q',-q}^p(\beta).$$

(22)

Using the Wigner-D expansion given in (21), we can write the alternative harmonic formulation of the SLSHT distribution component $g(\rho; \ell, m)$ in (18) as

$$g(\rho; \ell, m) = \sum_{p=0}^{L_h} \sum_{q=-p}^{p} \sum_{q'=-p}^{p} \overline{\left(\overline{f} Y_\ell^m\right)_p^q} (h)_p^{q'} i^{q-q'} \\ \times \sum_{q''=-p}^{p} \Delta_{q''q}^p \Delta_{q''q'}^p e^{-iq\alpha - iq''\beta - q'\gamma},$$

(23)

where $\rho = (\alpha, \beta, \gamma)$. By reordering the summations we can write

$$g(\rho; \ell, m) = \sum_{q=-L_h}^{L_h} \sum_{q'=-L_h}^{L_h} \sum_{q''=-L_h}^{L_h} C_{q,q',q''}(\ell, m) \\ \times e^{-iq\alpha - iq''\beta - q'\gamma}, \quad \rho = (\alpha, \beta, \gamma),$$

(24)

where

$$C_{q,q',q''}(\ell, m) = i^{q-q'} \sum_{p=\max(|q|,|q'|,|q''|)}^{L_h} \Delta_{q''q}^p \Delta_{q''q'}^p \overline{\left(\overline{f} Y_\ell^m\right)_p^q} (h)_p^{q'}.$$

Comparatively, the computation of the SLSHT distribution components using the expression given by (24) is not more efficient than the initial expression (19). However, the presence of complex exponentials can be exploited by employing FFTs to evaluate the involved summations.

The objective of factoring the rotations is to carry out the β rotation along the y-axis as a rotation along the z-axis. The rotations along the z-axis are expressed using complex exponentials and thus these rotations can be applied with much less computational burden, by exploiting the power of an FFT, relative to a rotation about the y-axis. All the three rotations which characterize the spatial domain of the SLSHT distribution components appear in complex exponentials in (24) and thus we can use FFTs to evaluate the summation of $C_{q,q',q''}(\ell, m)$ over q, q' and q''. First we need to compute $C_{q,q',q''}(\ell, m)$ for each ℓ and for each m which requires the one-dimensional summation over three dimensional grid formed by q, q' and q'' and thus can be computed in $O(L_h^4)$. Using $C_{q,q',q''}(\ell, m)$, the summation over the complex exponentials in (24) can be carried out in $O(L_h^3 \log_2 L_h)$ using FFTs. The overall complexity of this approach is dominated by the computation of $C_{q,q',q''}(\ell, m)$, that is, $O(L_h^4)$ for each SLSHT distribution component and $O(L_f^2 L_h^4)$ for the complete SLSHT distribution. We note that the evaluation of $C_{q,q',q''}(\ell, m)$ requires the computation of $\Delta_{qq'}^p$ which can be evaluated over the (q, q') plane for each p using the recursion formula of [46] with a complexity of $O(L_h^2)$. The Δ matrices are independent of the signal under analysis and therefore can be computed offline. However, we compute Δ matrices on-the-fly to minimize storage requirements. Since p is of the order L_h, the Δ matrices can be evaluated in $O(L_h^3)$, which does

not change the overall complexity of our proposed algorithm. The overall asymptotic complexity of our fast algorithm is thus $O(L_f^3 L_h^2 + L_f^2 L_h^4)$.

Remark 5: Since the complexity to compute the spherical harmonic transform of the modulated signal $\overline{f} Y_\ell^m$ up to degree L_h is $O(L_f^2 \log_2 L_f + L_f L_h^2)$ for each ℓ, m as shown in Appendix A, the complexity of our fast algorithm to compute one SLSHT distribution component is $O(L_f^2 \log_2 L_f + L_f L_h^2 + L_h^4)$. The factor $L_f^2 \log_2 L_f$ in the complexity does not change if we compute spherical harmonic transform of $\overline{f} Y_\ell^m$ up to degree L_h for all ℓ, m instead of each ℓ, m.

Remark 6: In order to evaluate (19), we note that the separation of variables approach [21] can be used as an alternative to the factoring of rotation approach to develop a fast algorithm. This is due to the factorized form of Wigner-D function and the consideration of equiangular tessellation scheme for SO(3), which keeps the independence between the samples along different Euler angles. In terms of the computational complexity, the separation of variable approach has the same computational complexity as the factoring of rotation approach. However, the separation of variable approach needs to compute Wigner-d functions for all values of β but only requires a two dimensional FFT, whereas the factoring of rotation approach only requires the evaluation of Wigner-d function for $\pi/2$ but requires a three dimensional FFT. Since both approaches have the same complexity, we use the factoring of rotation in our implementation of the fast algorithm.

Remark 7: If we want to analyze the signal f with multiple window functions, then we do not need to recalculate the spherical harmonic transform of the modulated signal $\overline{f} Y_\ell^m$, which accounts for the $O(L_f^3 L_h^2)$ factor in the overall complexity. Once it is computed, the SLSHT distribution can be computed in $O(L_f^2 L_h^4)$ time for each window function of the same band-limit using the proposed efficient implementation.

Our proposed formulation and efficient implementation can be further optimized in the case of a steerable window function. Steerable functions have an azimuthal harmonic band-limit in m that is less than the band-limit in ℓ (see [20], [21] for further details about steerability on the sphere). In this case, the $L_f^2 L_h^4$ factor contributing to the overall asymptotic complexity of the fast algorithm is reduced to $L_f^2 L_h^3$. Furthermore, we may then compute the directional SLSHT for any continuous $\gamma \in [0, 2\pi)$ from a small number of basis orientations (due to the linearity of the SLSHT).

If the signal and window function are real, the computational time can be further reduced by considering the conjugate symmetry relation of the spherical harmonic coefficients. Furthermore, in this setting, the SLSHT distribution components also satisfy the conjugate symmetry property

$$g(\rho; \ell, -m) = (-1)^m \overline{g(\rho; \ell, m)} \qquad (25)$$

and we do not need to compute the SLSHT distribution components of negative orders.

V. RESULTS

In this section, we first demonstrate the numerical validation and computation time of our algorithms to evaluate the directional SLSHT components. Later, we provide an example to illustrate the capability of the directional SLSHT, showing that it reveals the directional features of signals in the spatio-spectral domain. The implementation of the our algorithms is carried out in MATLAB, using the MATLAB interface of the SSHT[3] package (the core algorithms of which are written in C and which also uses the FFTW[4] package to compute Fourier transforms) to efficiently compute forward and inverse spherical harmonic transforms [35].

A. Numerical Validation and Computation Time

In order to evaluate the numerical accuracy and the computation time, we carry out the following numerical experiment. We use the band-limited function h for spatial localization with band-limit $L_h = 18$ and spatial localization in the region $\mathscr{R}_{(\pi/6, \pi/6 + \pi/240)}$. We generate band-limited test signals with band-limits $18 \le L_f \le 130$ by generating spherical harmonic coefficients with real and imaginary parts uniformly distributed in the interval $[0, 1]$.

For the given test signal, we measure the computation time τ_1 to evaluate spherical harmonic transform of the modulated signal, i.e., $(\overline{f} Y_\ell^m)_p^q$ for $p \le L_h$, $q \le |p|$ and for all $\ell \le L_f + L_h$, $m \le |\ell|$, using the method presented in Appendix A. Given the spherical harmonic transform of the modulated signal, we then measure the computation time τ_2 to compute all directional SLSHT distribution components $g(\rho; \ell, m)$ for $\ell \le L_f + L_h$ and $m \le |\ell|$ using our fast algorithm presented in Section IV-B, where we compute the Wigner-d functions on-the-fly for the argument $\pi/2$ by using the recursion of Trapani [46]. We also record the computation time τ_3 to recover a signal from its SLSHT distribution components. All numerical experiments are performed using MATLAB running on a 2.4 GHz Intel Xeon processor with 64 GB of RAM and the results are averaged over ten test signals. The computation time τ_1 and τ_2 are plotted against the band-limit L_f of the test signal in Fig. 1a and Fig. 1b, which respectively evolve as $O(L_f^3)$ and $O(L_f^2)$ for fixed L_h and thus corroborate the theoretical complexity. The computation time τ_3 for the inverse directional SLSHT is plotted in Fig. 1c, which scales as $O(L_f^2)$ for fixed L_h, again supporting the theoretical complexity.

We reconstruct the original signal from its SLSHT distribution components using (15) and (12), in order to assess the numerical accuracy of our algorithms by measuring the maximum absolute error between the original spherical harmonic coefficients of the test signal and the reconstructed values. The maximum absolute error is plotted in Fig. 1d for different band-limits L_f, which illustrates that our algorithms achieve very good numerical accuracy with numerical errors at the level of floating point precision.

B. Directional SLSHT Illustration

In this subsection, we provide examples to illustrate the capability of the proposed transform to reveal the localized
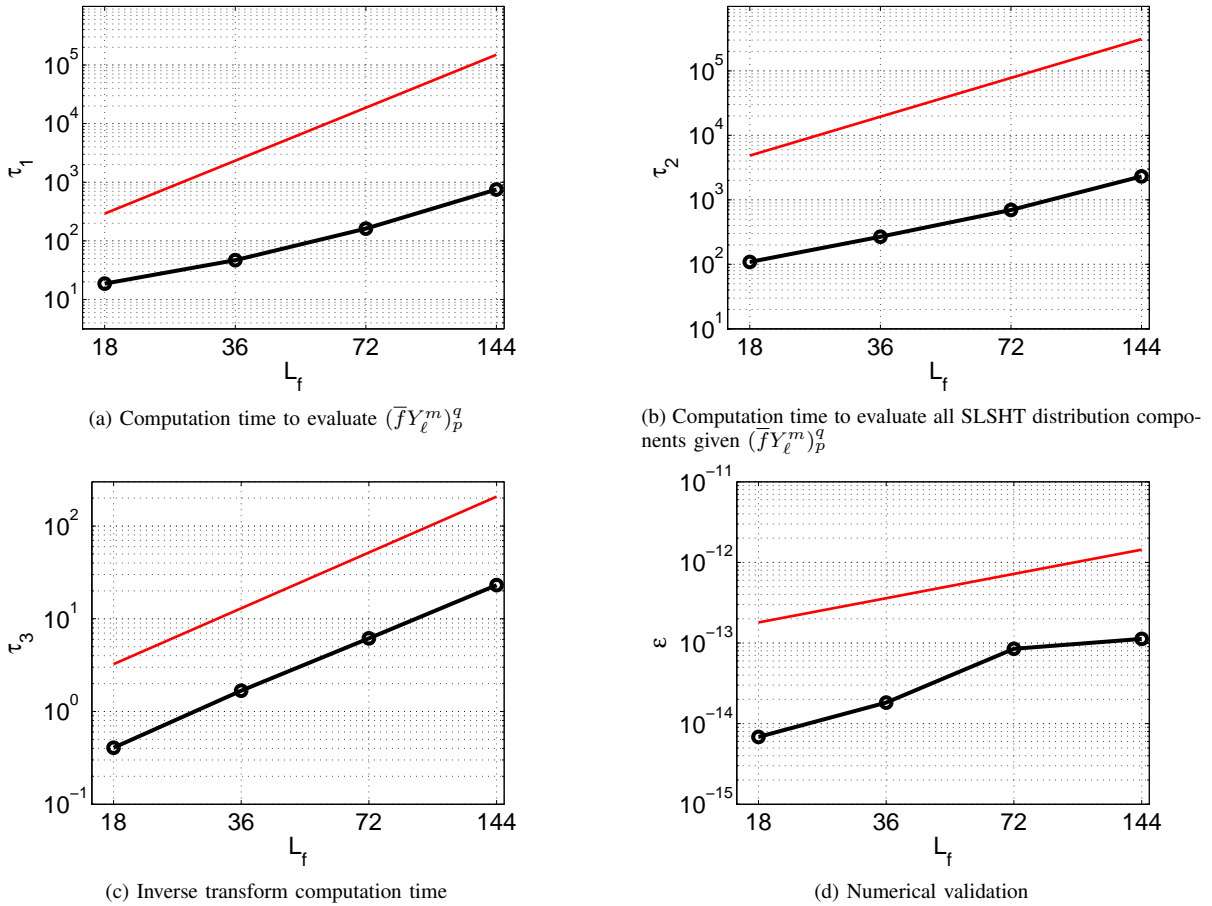
---

[3]http://www.jasonmcewen.org/
[4]http://www.fftw.org/

(a) Computation time to evaluate $(\overline{f}Y_\ell^m)_p^q$

(b) Computation time to evaluate all SLSHT distribution components given $(\overline{f}Y_\ell^m)_p^q$

(c) Inverse transform computation time

(d) Numerical validation

Fig. 1: Numerical validation and computation time of the proposed algorithms. The computation time in seconds: (a) τ_1 (b) τ_2 and (c) τ_3. For fixed L_h, τ_1 evolves as $O(L_f^3)$ and both τ_2 and τ_3 scale as $O(L_f^2)$ as shown by the solid red lines (without markers). (d) The maximum error ϵ, which empirically appears to scale as $O(L)$, as shown by the solid red line.

(a) f_1 (b) f_2 (c) f
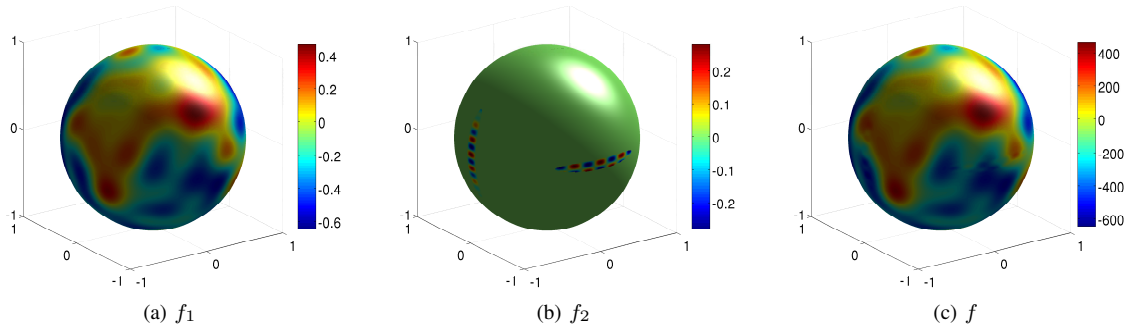
Fig. 2: (a) Spectrally truncated unit energy normalized Earth topographic map f_1 and (b) signal f_2 composed of higher degree spherical harmonics localized in elliptical regions. (c) Weighted sum of f_1 and f_2 as defined in (27)

.

contribution of spectral contents and probe the directional features in the spatio-spectral domain.

1) Example 1 - Synthetic Data Set: We first construct a signal having localized contribution of higher degree spectral contents and then analyze the signal using proposed directional SLSHT. Let signal f_1 be the spectrally truncated, unit energy normalized Earth topographic map with band-limit $L_{f_1} = 30$, which is obtained by using spherical harmonic model of topography of Earth and is shown in Fig. 2a. Also consider the signal f_2 composed of higher degree spherical harmonics localized in two non-overlapping elliptical regions with different orientation. We obtain such a signal f_2 by spectrally truncating the following signal $\tilde{f}_2$ with in the band-

limit $L_{f_2} = 128$,

$$
\tilde{f}_2(\hat{\boldsymbol{x}}) = \begin{cases} \sum_{\ell=40}^{45} \left(Y_\ell^{20}(\hat{\boldsymbol{x}}) + Y_\ell^{-20}(\hat{\boldsymbol{x}}) \right) & \hat{\boldsymbol{x}} \in \mathscr{R} = \mathscr{R}_1 \cup \mathscr{R}_1 \\ 0 & \hat{\boldsymbol{x}} \in \mathbb{S}^2 \setminus \mathscr{R}, \end{cases}
\tag{26}
$$

where $\mathscr{R}_1$ and $\mathscr{R}_2$ are the elliptical regions of the form $\mathscr{R}_{(\pi/6,\pi/6+\pi/240)}$, respectively rotated by $(\pi/2, \pi/2, 0) \in$ SO(3) and $(3\pi/2, \pi/2, \pi/2) \in$ SO(3). The unit energy normalized signal f_2 is shown in Fig. 2b. We note that the regions $\mathscr{R}_1$ and $\mathscr{R}_2$ have orientation along colatitude and longitude respectively.

We analyze the following synthetic signal using the proposed transform

$$f(\hat{\boldsymbol{x}}) = 10^3 \times \left(\frac{f_1(\hat{\boldsymbol{x}})}{\|f_1\|} + \frac{f_2(\hat{\boldsymbol{x}})}{4\|f_2\|} \right), \qquad (27)$$

which can be considered as a sum of low frequency signal and high frequency localized signal. The signal f is shown in Fig. 2c, where it can be observed that the information cannot be obtained about the presence of higher degree spherical harmonics localized in different directional regions. Furthermore, the spherical harmonic coefficients provide details about the presence of higher degree spherical harmonics in the signal, but do not reveal any information about the localized contribution of higher degree spherical harmonics.

If we analyze the signal by employing the SLSHT using an azimuthally symmetric window function, the presence of localized contributions of higher degree spectral contents can be determined in the spatio-spectral domain [10]. However, the presence of directional features cannot be extracted. Here, we illustrate that the use of the directional SLSHT enables the identification of directional features in the spatio-spectral domain, which is due to the consideration of an asymmetric window function for spatial localization.

We obtain the directional SLSHT distribution components $g(\rho; \ell, m)$ of the signal f using the band-limited eigenfunction window h with $L_h = 18$ and 90% concentration in the spatial domain in an elliptical region $\mathscr{R}_{(\pi/6, \pi/6+\pi/240)}$. The magnitude of the SLSHT distribution components $g(\rho; \ell, m)$ for order $m = 20$ and for degrees $\ell \in \{41, 43, 45\}$ are shown in Fig. 3 for Euler angle (a) $\gamma = 0$ and (b) $\gamma = 100\pi/201 \approx \pi/2$, and for degrees $\ell \in \{21, 23, 25\}$, the components are shown for (c) $\gamma = 0$ and (d) $\gamma \approx \pi/2$. Since the elliptical region is oriented along the x-axis, the window with orientation $\gamma = 0$ provides localization along colatitude and the window with orientation $\gamma \approx \pi/2$ provides localization along longitude. It can be observed that the localized contribution of higher degree directional spectral contents is extracted in spatio-spectral domain. The localized higher degree directional features along the orientation $\gamma = 0$ and $\gamma \approx \pi/2$ are revealed in the spatio-spectral domain as shown in Fig. 3a and Fig. 3b respectively, which are not visible in lower degree distribution components as shown in Fig. 3c and Fig. 3d.

Due to the ability of the directional SLSHT to reveal the localized contribution of spectral contents and the directional or oriented features in the spatio-spectral domain, it can be useful in many applications where the signal on the sphere is localized in position and orientation. We further illustrate the capability of our proposed transform by analyzing the Mars topographic map in spatio-spectral domain

2) Example 2 - Mars Data Set: Now, we consider the Mars topographic map (height above geoid) as a signal on the sphere, which is obtained by using the spherical harmonic model of the topography of Mars[5]. The Mars topographic map is shown in Fig. 4 in the spatial domain, where the grand canyon Valles Marineris and the mountainous regions of Tharsis Montes and Olympus Montes are shown, leading
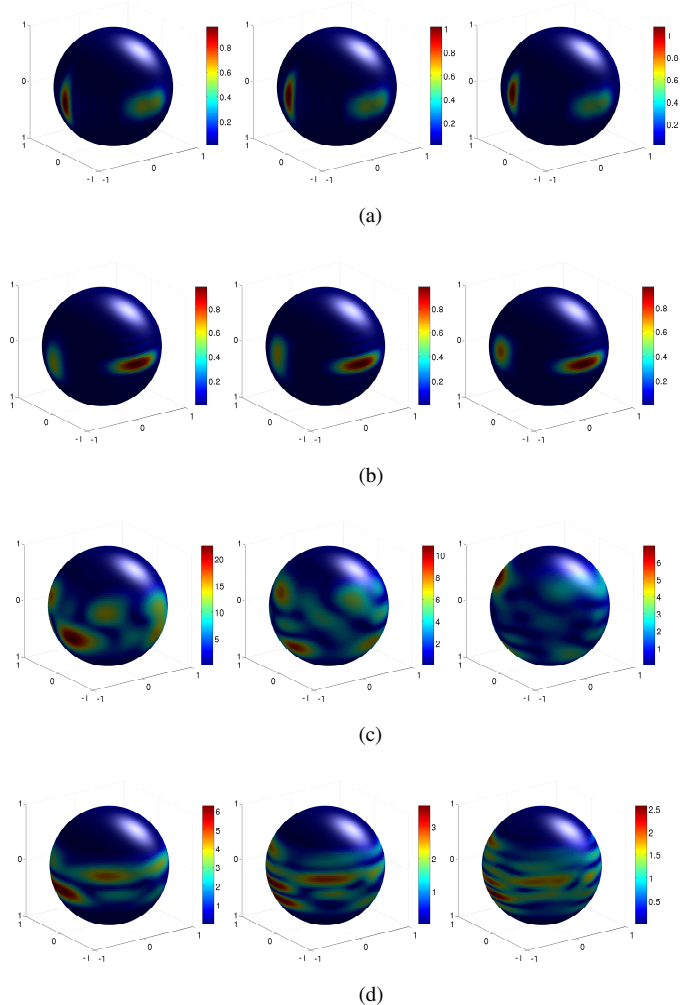
[5]http://www.ipgp.fr/~wieczor/SH/

(a)

(b)

(c)

(d)

Fig. 3: Magnitude of the components of the directional SLSHT distribution of the synthetic signal shown in Fig. 2c. For fixed orientation γ of the window function around z-axis, the distribution components $g(\rho; \ell, m)$ are mapped on the sphere using $\rho = (\phi, \theta, \gamma)$ for order $m = 20$. The components are shown for degrees $\ell \in \{41, 43, 45\}$ and for orientation (a) $\gamma = 0$ and (b) $\gamma \approx \pi/2$ of the window function around z-axis, and the components are shown for degrees $\ell \in \{21, 23, 25\}$ and for orientation (c) $\gamma = 0$ and (d) $\gamma \approx \pi/2$. Top left: $g(\rho; 41, 20)$, top right: $g(\rho; 45, 20)$.

to the high frequency contents. We note that the mountainous regions are non-directional features of the Mars map, whereas the grand canyon serves as a directional feature with direction orientated along a line of approximate constant latitude.

The directional SLSHT distribution components $g(\rho; \ell, m)$ of the Mars map f are obtained using the band-limited eigenfunction window h with $L_h = 60$ and 90% concentration in the spatial domain in an elliptical region $\mathscr{R}_{(\pi/16, \pi/15)}$. The magnitude of the SLSHT distribution components $g(\rho; \ell, m)$ for order $m = 15$ and degrees $80 \le \ell \le 85$ and $20 \le \ell \le 25$ are shown in Fig. 5a and Fig. 5b respectively for $\gamma \approx \pi/2$. It is evident that using orientation of the window $\gamma \approx \pi/2$ probes the information about the grand canyon Valles Marineris (directional feature) along longitude in the spatio-spectral domain. The localized contribution of higher degree
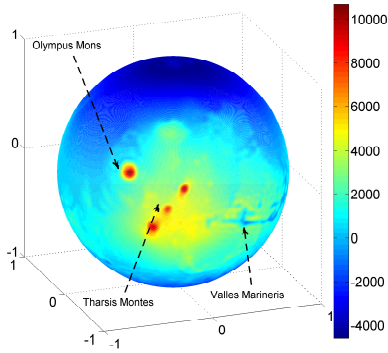
Fig. 4: Mars signal in the spatial domain. The grand canyon Valles Marineris and the mountainous regions of Tharsis Montes and Olympus Montes are indicated.

spherical harmonics towards the mountainous region can also be observed in Fig. 5b for degree $20 \leq \ell \leq 25$. However, there is no significant contribution of spherical harmonics of degree $80 \leq \ell \leq 85$ towards mountainous region as indicated in Fig. 5a, but the localization of the directional features along the orientation $\gamma \approx \pi/2$ is revealed in the spatio-spectral domain.

VI. CONCLUSIONS

We have presented the directional SLSHT to project a signal on the sphere onto its joint spatio-spectral domain as a directional SLSHT distribution. In spirit, the directional SLSHT is composed of SO(3) spatial localization followed by the spherical harmonic transform. Here, we have proposed the use of an azimuthally asymmetric window function to obtain spatial localization, which enables the transform to resolve directional features in the spatio-spectral domain. We have also presented an inversion relation to synthesize the original signal from its directional SLSHT distribution. Since data-sets on the sphere are of considerable size, we have developed a fast algorithm for the efficient computation of the directional SLSHT distribution of a signal. The computational complexity of computing the directional SLSHT is reduced by providing an alternative harmonic formulation of the transform and then exploiting the factoring of rotation approach [44] and the fast Fourier transform. The computational complexity of the proposed fast algorithm to evaluate SLSHT distribution of a signal with band-limit L_f using window function with band-limit L_h is $O(L_f^3 L_h^2 + L_f^2 L_h^4)$ as compared to the complexity of direct evaluation, which is $O(L_f^4 L_h^3)$. The numerical accuracy and the speed of our fast algorithm has also been studied. The directional SLSHT distribution relies on a window function for spatial localization; we have analyzed the band-limited window function obtained from the Slepian concentration problem on the sphere, with nominal concentration in an elliptical region around the north pole. We provided an illustration which highlighted the capability of the directional SLSHT to reveal directional features in the spatio-spectral domain, which is likely to be of use in many applications.
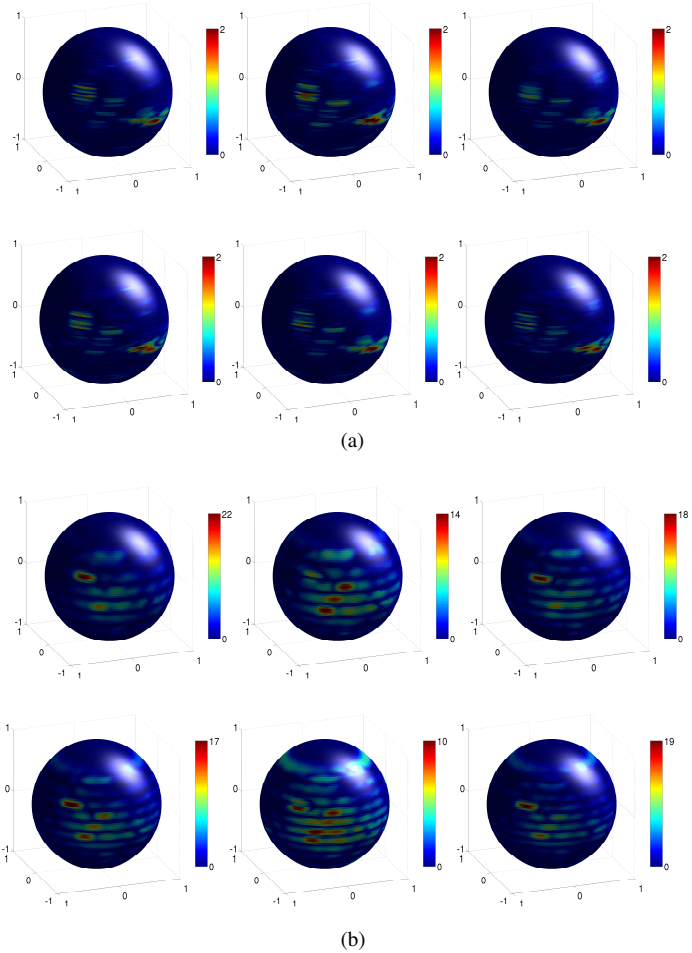

(a)

(b)

Fig. 5: Magnitude of the components of the directional SLSHT distribution of the Mars signal obtained using the eigenfunction window concentrated in an elliptical region of focus $\theta_c = \pi/16$ and major axis $a = \pi/15$. For fixed orientation γ, the distribution components $g(\rho; \ell, m)$ are mapped on the sphere using $\rho = (\phi, \theta, \gamma)$ for order $m = 15$ and degrees (a) $80 \leq \ell \leq 85$ and (b) $20 \leq \ell \leq 25$. The components are shown for orientation $\gamma \approx \pi/2$ of the window function around the z-axis. Top left: $g(\rho; 20, 15)$, top right: $g(\rho; 22, 15)$.

APPENDIX A
SPHERICAL HARMONIC TRANSFORM OF MODULATED SIGNAL

Our objective is to compute the spherical harmonic transform of the modulated signal $\overline{f} Y_\ell^m$, up to degree L_h, for all ℓ and m. In order to serve the purpose, we use a separation variable technique given by

$$\left(\overline{f} \, Y_\ell^m\right)_p^q = N_\ell^m N_p^q \int_0^\pi P_\ell^m(\cos\theta) P_p^q(\cos\theta)$$
$$\times \underbrace{\int_0^{2\pi} \overline{f(\theta,\phi)} e^{i(m-q)\phi} d\phi}_{I(\theta, m-q)} \sin\theta d\theta. \qquad (28)$$

Since $0 \leq \ell \leq L_f + L_h$ and $0 \leq p \leq L_h$, we need to consider the signal $\overline{f} \, Y_\ell^m$ sampled on the grid $\mathfrak{S}_{2L_f + 2L_h}$ for the explicit evaluation of exact quadrature (note that sampling in ϕ could be optimized given $|m - q| \leq L_f + 2L_h$ but this would require a different tessellation of the sphere and will not

alter the overall complexity of the computation). Using (28), the integral over ϕ, giving $I(\theta, m - q)$, can be computed first in $O(L_f^2 \log_2 L_f)$ for all $m - q$. Once $I(\theta, m - q)$ is computed, the exact quadrature weights that follow from [35] can be used to evaluate the integral over θ in $O(L_f)$ for each p, q, ℓ, m and in $O(L_f L_h^2)$ for all p, q, and each ℓ, m. Thus the overall complexity to compute the spherical harmonic transform of the modulated signal $\overline{f} Y_\ell^m$ up to degree L_h is $O(L_f^2 \log_2 L_f + L_f L_h^2)$ for each ℓ, m and $O(L_f^2 \log_2 L_f + L_f^3 L_h^2) = O(L_f^3 L_h^2)$ for all ℓ, m.

REFERENCES

[1] M. K. Chung, K. J. Worsley, B. M. Nacewicz, K. M. Dalton, and R. J. Davidson, "General multivariate linear modeling of surface shapes using SurfStat," *NeuroImage*, vol. 53, no. 2, pp. 491–505, 2010.

[2] F. J. Simons, F. A. Dahlen, and M. A. Wieczorek, "Spatiospectral concentration on a sphere," *SIAM Rev.*, vol. 48, no. 3, pp. 504–536, 2006.

[3] C. Han, B. Sun, R. Ramamoorthi, and E. Grinspun, "Frequency domain normal map filtering," *ACM Trans. on Graphics*, vol. 26, no. 3, pp. 28:1–28:12, Jul. 2007.

[4] P. Audet, "Directional wavelet analysis on the sphere: Application to gravity and topography of the terrestrial planets," *J. Geophys. Res.*, vol. 116, Feb. 2011.

[5] D. Colton and R. Kress, *Inverse Acoustic and Electromagnetic Scattering Theory*, 2nd ed. Berlin: Springer-Verlag, 1998.

[6] D. N. Spergel, R. Bean *et al.*, "Three-year Wilkinson Microwave Anisotropy Probe (WMAP) observations: Implications for cosmology," *The Astrophysical Journal Supplement Series*, vol. 170, no. 2, pp. 377–408, 2007.

[7] D. B. Ward, R. A. Kennedy, and R. C. Williamson, "Theory and design of broadband sensor arrays with frequency invariant far-field beam patterns," *J. Acoust. Soc. Am.*, vol. 97, no. 2, pp. 1023–1034, Feb. 1995.

[8] T. S. Pollock, T. D. Abhayapala, and R. A. Kennedy, "Introducing space into MIMO capacity calculations," *J. Telecommun. Syst.*, vol. 24, no. 2, pp. 415–436, Oct. 2003.

[9] J.-P. Antoine and P. Vandergheynst, "Wavelets on the 2-sphere: A group-theoretical approach," *Appl. Comput. Harmon. Anal.*, vol. 7, no. 3, pp. 262–291, 1999.

[10] Z. Khalid, S. Durrani, P. Sadeghi, and R. A. Kennedy, "Spatio-spectral analysis on the sphere using spatially localized spherical harmonics transform," *IEEE Trans. Signal Process.*, vol. 60, no. 3, pp. 1487–1492, Mar. 2012.

[11] Z. Khalid, S. Durrani, R. A. Kennedy, and P. Sadeghi, "Conjugate gradient algorithm for extrapolation of sampled bandlimited signals on the 2-sphere," in *Proc. IEEE Int. Conf. Acoust., Speech, Signal Process., ICASSP'2012*, Kyoto, Japan, Mar. 2011.

[12] Z. Khalid, P. Sadeghi, R. A. Kennedy, and S. Durrani, "Spatially varying spectral filtering of signals on the unit sphere," *IEEE Trans. Signal Process.*, vol. 61, no. 3, pp. 530–544, Feb. 2013.

[13] D. Marinucci, D. Pietrobon *et al.*, "Spherical needlets for cosmic microwave background data analysis," *Mon. Not. R. Astron. Soc.*, vol. 383, no. 2, pp. 539–545, 2008.

[14] J. D. McEwen, M. P. Hobson, and A. N. Lasenby, "A directional continuous wavelet transform on the sphere," *Arxiv preprint astro-ph/0609159*, 2006.

[15] J. D. McEwen, M. P. Hobson, D. J. Mortlock, and A. N. Lasenby, "Fast directional continuous spherical wavelet transform algorithms," *IEEE Trans. Signal Process.*, vol. 55, no. 2, pp. 520–529, Feb. 2007.

[16] J. D. McEwen, M. P. Hobson, and A. N. Lasenby, "Optimal filters on the sphere," *IEEE Trans. Signal Process.*, vol. 56, no. 8, pp. 3813–3823, Aug. 2008.

[17] P. Sadeghi, R. A. Kennedy, and Z. Khalid, "Commutative anisotropic convolution on the 2-sphere," *IEEE Trans. Signal Process.*, vol. 60, no. 12, pp. 6697–6703, Dec. 2012.

[18] M. Simons, S. C. Solomon, and B. H. Hager, "Localization of gravity and topography: constraints on the tectonics and mantle dynamics of Venus," *Geophys. J. Int.*, vol. 131, no. 1, pp. 24–44, Oct. 1997.

[19] J.-L. Starck, Y. Moudden, P. Abrial, and M. Nguyen, "Wavelets, ridgelets and curvelets on the sphere," *Astron. & Astrophys.*, vol. 446, no. 3, pp. 1191–1204, Feb. 2006.

[20] Y. Wiaux, L. Jacques, and P. Vandergheynst, "Correspondence principle between spherical and Euclidean wavelets," *Astrophys. J.*, vol. 632, no. 1, pp. 15–28, Oct. 2005.

[21] Y. Wiaux, L. Jacques, P. Vielva, and P. Vandergheynst, "Fast directional correlation on the sphere with steerable filters," *Astrophys. J.*, vol. 652, no. 1, pp. 820–832, Nov. 2006.

[22] Y. Wiaux, J. D. McEwen, P. Vandergheynst, and O. Blanc, "Exact reconstruction with directional wavelets on the sphere," *Mon. Not. R. Astron. Soc.*, vol. 388, no. 2, pp. 770–788, 2008.

[23] B. T. T. Yeo, W. Ou, and P. Golland, "On the construction of invertible filter banks on the 2-sphere," *IEEE Trans. Image Process.*, vol. 17, no. 3, pp. 283–300, Mar. 2008.

[24] R. B. Barreiro, M. P. Hobson *et al.*, "Testing the Gaussianity of the COBE DMR data with spherical wavelets," *Mon. Not. R. Astron. Soc.*, vol. 318, pp. 475–481, Oct. 2000.

[25] J. D. McEwen, M. P. Hobson, A. N. Lasenby, and D. J. Mortlock, "A high-significance detection of non-Gaussianity in the Wilkinson Microwave Anisotropy Probe 1-yr data using directional spherical wavelets," *Mon. Not. R. Astron. Soc.*, vol. 359, no. 4, pp. 1583–1596, 2005.

[26] J. D. McEwen, P. Vielva *et al.*, "Cosmological applications of a wavelet analysis on the sphere," *J. Fourier Anal. Appl.*, vol. 13, no. 4, pp. 495–510, Aug. 2007.

[27] D. Pietrobon, A. Amblard *et al.*, "Needlet detection of features in the WMAP CMB sky and the impact on anisotropies and hemispherical asymmetries," *Phys. Rev. D*, vol. 78, no. 10, p. 103504, Nov. 2008.

[28] J. Schmitt, J.-L. Starck, J. M. Casandjian, J. Fadili, and I. Grenier, "Poisson denoising on the sphere: application to the Fermi gamma ray space telescope," *Astron. & Astrophys.*, vol. 517, p. A26, Jul. 2010.

[29] P. Vielva, E. Martínez-González, R. B. Barreiro, J. L. Sanz, and L. Cayón, "Detection of non-Gaussianity in the WMAP 1-year data using spherical wavelets," *Astrophys. J.*, vol. 609, pp. 22–34, 2004.

[30] F. J. Simons, I. Loris *et al.*, "Solving or resolving global tomographic models with spherical wavelets, and the scale and sparsity of seismic heterogeneity," *Geophys. J. Int.*, vol. 187, pp. 969–988, 2011.

[31] F. J. Simons, I. Loris, E. Brevdo, and I. C. Daubechies, "Wavelets and wavelet-like transforms on the sphere and their application to geophysical data inversion," in *Wavelets and Sparsity XIV*, vol. 81380. SPIE, 2011, p. 81380X.

[32] M. A. Wieczorek and F. J. Simons, "Localized spectral analysis on the sphere," *Geophys. J. Int.*, vol. 162, no. 3, pp. 655–675, May 2005.

[33] M. A. Wieczorek and F. J. Simons, "Minimum variance multitaper spectral estimation on the sphere," *J. Fourier Anal. Appl.*, vol. 13, no. 6, pp. 665–692, 2007.

[34] J. R. Driscoll and D. M. Healy, Jr., "Computing Fourier transforms and convolutions on the 2-sphere," *Adv. Appl. Math.*, vol. 15, no. 2, pp. 202–250, Jun. 1994.

[35] J. D. McEwen and Y. Wiaux, "A novel sampling theorem on the sphere," *IEEE Trans. Signal Process.*, vol. 59, no. 12, pp. 5876–5887, Dec. 2011.

[36] J. J. Sakurai, *Modern Quantum Mechanics*, 2nd ed. Reading, MA: Addison Wesley Publishing Company, Inc., 1994.

[37] N. Jarosik, C. L. Bennett *et al.*, "Seven-year Wilkinson Microwave Anisotropy Probe (WMAP) observations: Sky maps, systematic errors, and basic results," *Astrophys. J.*, vol. 192, no. 2, pp. 1–14, 2011.

[38] Planck collaboration, "ESA Planck blue book," ESA, Tech. Rep. ESA-SCI(2005)1, 2005.

[39] R. A. Kennedy, T. A. Lamahewa, and L. Wei, "On azimuthally symmetric 2-sphere convolution," *Digital Signal Processing*, vol. 5, no. 11, pp. 660–666, Sep. 2011.

[40] D. A. Varshalovich, A. N. Moskalev, and V. K. Khersonskii, *Quantum Theory of Angular Momentum*. World Scientific, 1988.

[41] W. Freeden and V. Michel, "Constructive approximation and numerical methods in geodetic research today – an attempt at a categorization based on an uncertainty principle." *J. Geodesy*, vol. 73, no. 9, pp. 452–465, 1999.

[42] G. Jones and B. Boashash, "Window matching in the time-frequency plane and the adaptive spectrogram," in *Proceedings of the IEEE-SP International Symposium Time-Frequency and Time-Scale Analysis, 1992*, Oct. 1992, pp. 87–90.

[43] Z. Khalid, S. Durrani, R. A. Kennedy, and P. Sadeghi, "Revisiting Slepian concentration problem on the sphere for azimuthally non-symmetric regions," in *5th International Conference on Signal Processing and Communication Systems, ICSPCS'2011*, Honolulu, HI, Dec. 2011.

[44] T. Risbo, "Fourier transform summation of Legendre series and D-functions," *J. Geodesy*, vol. 70, pp. 383–396, 1996.

[45] B. D. Wandelt and K. M. Górski, "Fast convolution on the sphere," *Phys. Rev. D*, vol. 63, no. 12, p. 123002, May 2001.

[46] S. Trapani and J. Navaza, "Calculation of spherical harmonics and Wigner *d* functions by FFT. Applications to fast rotational matching in

molecular replacement and implementation into AMoRe," *Acta Cryst. A*, vol. 62, no. 4, pp. 262–269, Jul. 2006.

Zubair Khalid (S'10) received his B.Sc. (first-class hons.) degree in Electrical Engineering from the University of Engineering & Technology (UET), Lahore, Pakistan in 2008. He is currently pursuing his PhD degree from the Research School of Engineering, the Australian National University, Canberra, Australia. Zubair was awarded University Gold Medal and Industry Gold Medals from Siemens and Nespak for his overall outstanding performance in Electrical Engineering during the his undergraduate studies. He is a recipient of an Endeavour International Postgraduate Award for the duration of his Ph.D. He was also awarded an ANU Vice Chancellors Higher Degree Research (HDR) travel grant in 2011. His research interests are in the area of development of novel signal processing techniques for signals on the sphere.

Rodney A. Kennedy (S'86-M'88-SM'01-F'05) received the B.E. degree from the University of New South Wales, Sydney, Australia, the M.E. degree from the University of Newcastle, and the Ph.D. degree from the Australian National University, Canberra.

He is currently a Professor in the Research School of Engineering, Australian National University. He is a Fellow of the IEEE. His research interests include digital signal processing, digital and wireless communications, and acoustical signal processing.

Salman Durrani (S'00-M'05-SM'10) received the B.Sc. (1st class honours) degree in Electrical Engineering from the University of Engineering & Technology, Lahore, Pakistan in 2000. He received the PhD degree in Electrical Engineering from the University of Queensland, Brisbane, Australia in Dec. 2004. He has been with the Australian National University, Canberra, Australia, since 2005, where he is currently a Senior Lecturer in the Research School of Engineering, College of Engineering & Computer Science.

His current research interests are in wireless communications and signal processing, including synchronization in cooperative communication systems, connectivity of ad-hoc networks and vehicular networks and signal processing on the unit sphere. He serves as a Technical Program Committee Member for international conferences such as ICC '13, PIMRC '12 and AusCTW '12. He was awarded an ANU Vice-Chancellor's Award for Teaching Excellence in 2012. He was a recipient of an International Postgraduate Research Scholarship from the Australian Commonwealth during 2001-2004. He was awarded a University Gold Medal during his undergraduate studies. He has 55 publications to date in refereed international journals and conferences. He is a Member of Institution of Engineers, Australia and a Senior Member of IEEE.

Parastoo Sadeghi (S'02-M'06-SM'07) received the B.E. and M.E. degrees in electrical engineering from Sharif University of Technology, Tehran, Iran, in 1995 and 1997, respectively, and the Ph.D. degree in electrical engineering from The University of New South Wales, Sydney, Australia, in 2006. From 1997 to 2002, she worked as a Research Engineer and then as a Senior Research Engineer at Iran Communication Industries (ICI) in Tehran, Iran and at Deqx (formerly known as Clarity Eq) in Sydney, Australia. She is currently a Fellow at the Research School of Engineering, The Australian National University, Canberra, Australia. She has visited various research institutes, including the Institute for Communications Engineering, Technical University of Munich, from April to June 2008 and MIT from February to May 2009.

Dr. Sadeghi has co-authored more than 80 refereed journal or conference papers and is a Chief Investigator in a number of Australian Research Council Discovery and Linkage Projects. In 2003 and 2005, she received two IEEE Region 10 student paper awards for her research in the information theory of time-varying fading channels. Her research interests are mainly in the area of wireless communications systems and signal processing.

Yves Wiaux received the M.S. degree in physics and the Ph.D. degree in theoretical physics from the Université catholique de Louvain (UCL), Louvain-la-Neuve, Belgium, in 1999 and 2002, respectively.

He was a Postdoctoral Researcher at the Signal Processing Laboratories of the Ecole Polytechnique Fédérale de Lausanne (EPFL), Switzerland, from 2003 to 2008. He was also a Postdoctoral Researcher of the Belgian National Science Foundation (F.R.S.-FNRS) at the Physics Department of UCL from 2005 to 2009. He is now a Maître Assistant of the University of Geneva (UniGE), Switzerland, with joint affiliation between the Institute of Electrical Engineering and the Institute of Bioengineering of EPFL, and the Department of Radiology and Medical Informatics of UniGE. His research lies at the intersection between complex data processing (including development on wavelets and compressed sensing) and applications in astrophysics (notably in cosmology and radio astronomy) and in biomedical sciences (notably in structural and diffusion MRI).

Jason McEwen received a B.E. (Hons) degree in Electrical and Computer Engineering from the University of Canterbury, New Zealand, in 2002 and a Ph.D. degree in Astrophysics from the University of Cambridge in 2007.

He held a Research Fellowship at Clare College, Cambridge, from 2007 to 2008, worked as a Quantitative Analyst from 2008 to 2010, and held a position as a Postdoctoral Researcher at Ecole Polytechnique Fédérale de Lausanne (EPFL), Switzerland, from 2010 to 2011. From 2011 to 2012 he held a Leverhulme Trust Early Career Fellowship at University College London (UCL), where he remains as a Newton International Fellow, supported by the Royal Society and the British Academy. His research interests are focused on spherical signal processing, including sampling theorems and wavelets on the sphere, compressed sensing and Bayesian statistics, and applications of these techniques to cosmology and radio interferometry.